Effect of alpha and Gaussian refractive index profiles on the design of highly nonlinear optical fibre for efficient nonlinear optical signal processing

S. Selvendran, A. Sivanantharaja, S. Arivazhagan, M. Kannan

Abstract. **We propose an index profiled, highly nonlinear ultra-flattened dispersion fibre (HN-UFF) with appreciable values of fibre parameters such as dispersion, dispersion slope, effective area, nonlinearity, bending loss and splice loss. The designed fibre has normal zero flattened dispersion over S, C, L, U bands and extends up to 1.9857 μm. The maximum dispersion variation observed for this fibre is as low as 1.61 ps km^{-1} nm^{-1} over the 500-nm optical fibre transmission spectrum. This fibre also has two zero dispersion wavelengths at 1.487 and 1.9857 μm and the respective dispersion slopes are 0.02476 and 0.0068 ps nm^{-2} km^{-1}. The fibre has a very low ITU-T cutoff wavelength of 1.2613 μm and a virtuous nonlinear coefficient of 9.43 W^{-1} km^{-1}. The wide spectrum of zero flattened dispersion and a good nonlinear coefficient make the designed fibre very promising for different nonlinear optical signal processing applications.**

Keywords: refractive index profile, effective area, dispersion, dispersion slope, highly nonlinear ultra-flattened dispersion fibre, four-wave mixing.

1. Introduction

The increasing number of users in the communication sector requires a substantial increase in the data rate and bandwidth. Obviously, this demand can only be satisfied by optical communication. Even though optical communication enjoys more bandwidth than conventional communication systems, the traffic contention problem nowadays comes to the fore, which will aggravate the situation even more in the future due to a tremendous deployment of optical communication all over the world. In the future this issue may demand a new transmission window for optical communication. The traffic contention problem can be eliminated by the multicasting technique, which is nothing but replication of information to multiple selected destinations. In this connection, multicasting, which is implemented by the wavelength conversion technique, plays a key role and allows one to dynamically recon-

S. Selvendran, A. Sivanantharaja Alagappa Chettiar College of Engineering and Technology, Karaikudi, Tamilnadu, India;
e-mail: selvendrans@aol.com;
S. Arivazhagan Mepco Schlenk Engineering College, Sivakasi, Tamilnadu, India;
M. Kannan Madras Institute of Technology, Chennai, Tamilnadu, India

figure future ultra-dense wavelength division multiplexing (UDWDM) networks. Wavelength conversion makes it possible to effectively utilise the allocated bandwidth, similarly to the frequency reuse technique in mobile communication. In order to satisfy the bandwidth demand, a new transmission window can be opened up with the use of advanced optical components (multi-wavelength laser sources based optical nonlinearity) and different optical fibres with other associated components.

An ultrafast all-optical signal processing is a promising technology used to overcome the problems of optical-to-electrical-to-optical conversion and support for the high bitrate operation [1]. All-optical nonlinear signal processing can be achieved with the help of third-order optical susceptibility nonlinear phenomena such as self-phase modulation (SPM), cross-phase modulation (XPM), four-wave mixing (FWM) and Raman scattering [2]. Among this FWM is an important phenomenon which is mainly used for wavelength conversion, parametric amplification and supercontinuum generation due to the transparent nature of bitrate, phase and modulation formats in newly generated signals. In addition, FWM also preserves the signal-to-noise ratio [2]. In a FWM process, two waves with frequencies ω_1 and ω_2 propagating in a nonlinear medium generate two new frequency components $\omega_3 \approx (2\omega_1 - \omega_2)$ and $\omega_4 \approx (2\omega_2 - \omega_1)$, where ω_3 and ω_4 are transparent signals of ω_2 and ω_1.

Highly nonlinear fibre (HNLF), semiconductor optical amplifier (SOA) and silica waveguides are practical candidates for nonlinear optical signal processing [3, 4]. HNLF is more preferable compared to other media because it has an ultrafast response time, low noise figure, passivity (no power consumption) and wide and flat band conversion [3]. The requirement to the HNLF design is a small effective area of the core (for high nonlinearity), right amount of dispersion according to versatile applications, low polarisation mode dispersion (PMD), low attenuation (to increase the effective interaction length) and, finally, the cutoff wavelength should be much shorter than the wavelength operated [5]. In the wavelength conversion technique the quality of the converted signal can be determined by the conversion efficiency and bit error rate (BER) [6]. The performance of HNLF is determined by the effective bandwidth utilisation of fibre, i.e. the difference between the wavelengths at which the conversion efficiency falls below 3 dB from the maximum value [7]. In general, HNLF ensures a high conversion efficiency at a zero dispersion wavelength (λ_{ZDW}) and drastically decreases for the wavelength far from the λ_{ZDW} due to an increase in phase mismatch between the signals by the dispersion profile [7, 8]. If we reduce the dispersion and dispersion slope to a very

minimal value and flatten the dispersion curve near to zero over the wavelength spectrum then we can increase the effective bandwidth utilisation of this fibre [8]. The dispersion curve flatness with good nonlinearity can improve the phase matching condition between the signals which are located far from the λ_{ZDW}; thereby, the conversion efficiency can also be improved at these wavelengths. Thus, we can also flatten the conversion efficiency over a wide wavelength spectrum. The conversion efficiency [9] of the newly generated signal using the FWM technique in HNLF is given by the equation

$$\eta = \frac{\alpha^2}{\alpha^2 + \Delta\beta^2}\left[1 + \frac{4\exp(-\alpha L)\sin^2(\Delta\beta L/2)}{[1 - \exp(-\alpha L)]^2}\right],\qquad(1)$$

where L is the fibre length, and α is the loss coefficient. The propagation constant differences Δ associated with wave generation at ω_3 and ω_4 are expressed as

$$\Delta\beta(\omega_3) = 2\beta\omega_1 - \beta\omega_2 - \beta\omega_3,$$

$$\Delta\beta(\omega_4) = 2\beta\omega_2 - \beta\omega_1 - \beta\omega_4.$$

By reducing $\Delta\beta$, as stated earlier, the phase matching condition between the input signal at ω_1 and ω_2 can be improved and we can increase the mutual interaction (reduce the walkoff) between the input signals in order to transfer a maximum power to newly generated signals. The FWM conversion efficiency [6] is optimum if $\Delta\beta = 0$. It is quite difficult to attain in practice; however, we can try to reach this with the help of a specifically designed fibre, which should have a uniformly distributed very-low dispersion over the broad range of the optical spectrum. It will allow $\Delta\beta$ to be nearly zero. As we can see from the equation below

$$\Delta\beta(\omega_3, \omega_4) \approx 2\pi c \frac{\Delta\lambda^2}{\lambda_m^2}\left[D(\lambda_m) \pm \frac{\Delta\lambda}{2}\frac{dD}{d\lambda}\bigg|_{\lambda_m}\right]\qquad(2)$$

(the plus and minus signs are used for $\Delta\beta(\omega_3)$ and $\Delta\beta(\omega_4)$, respectively; c is the speed of light; λ_m is the mean wavelength; and $\Delta\lambda = \lambda_1 - \lambda_2$), by reducing the dispersion D we can enhance the FWM interaction [9]. The total dispersion of the fibre is the sum of material and waveguide dispersions. The material dispersion is fixed, such that the total dispersion with respect to the wavelength can be modified (or reduced to zero) by the modifying the waveguide dispersion with a negative value. The waveguide dispersion can be adjusted through a change in the refractive index profile of fibre. Hence, the detrimental effect of FWM is the dependence of the conversion efficiency on the input signal frequency spacing, which can be overcome as much as possible by flattening and attenuating the fibre dispersion. The index profile optimisation can also useful for designing a fibre with more than one λ_{ZDW}. Such a fibre along with a flattened zero dispersion curve is promising for such nonlinear applications as supercontinuum generation.

Various step and graded index profile fibres were designed and reported previously by many authors [10–17]. In this paper, we have designed and optimised a double-clad-type HNLF (Fibre C) with ultra-flattened normal zero dispersion effects for the future optical signal processing. The alpha-peak and Gaussian index profiles are used for estimating the electrical field distribution of the designed fibre. The resultant

fibre design also has a low effective area, bending loss and splice loss. The simulation results show that our newly designed fibre is a better alternative to handle high bandwidth and multiple high bitrate wavelength channels in nonlinear optical signal processing. The ultra-flattened dispersion response obtained from such fibres enables the FWM conversion efficiency to be constant for wavelength conversion applications [7, 14]. It also increases the parametric gain bandwidth and supercontinuum spectral width.

2. Design of optimised HN-UFF fibre

In designing a highly nonlinear ultra-flattened dispersion fibre (HN UFF) we used the alpha power law function and Gaussian index profile approximation. In the alpha power law function, the alpha-power dependence has two forms: alpha peak and alpha dip [18]. In our simulation, we introduce the alpha-peak profile for the core and the Gaussian profile for the next depressed cladding layer [see Fig. 1 and Eqn (3)]. Due to the graded index structure of the alpha-peak core and by optimising the index parameters of the core, we can reduce the chromatic dispersion and maintain it flat over a broad range of the spectrum. This reduced flattened dispersion characteristics can increase the utilisation bandwidth of the optical fibre [19, 20]. The alpha-peak core also enhances the optical confinement to the centre of the core, which increases nonlinearity and lowers the cutoff wavelength in our designed fibres. In addition, the Gaussian profile of the cladding adjacent to the core allows a tremendous improvement in dispersion flattened characteristics of
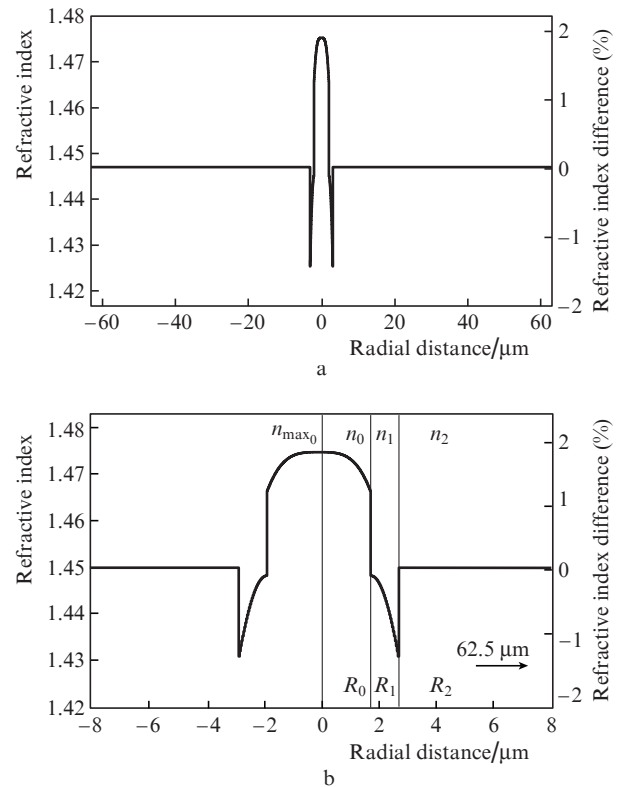

Figure 1. (a) Refractive index profile of the proposed optimised HN-UFF (Fibre C) and (b) magnified view of a part of the profile.

fibre. The Gaussian profile [21–23] with its optimised refractive index and full width at half maximum (FWHM) values allow a further reduction in the dispersion slope and effective area. The other fibre performance parameters such as splice loss, cutoff wavelength and polarisation mode dispersion (PMD) are optimised by varying both alpha and Gaussian parameters.

The refractive index profile of the proposed fibre and its magnified view are shown in Fig. 1. The refractive index n of this profile as a function of the radial distance r are derived from the equation

$$n(r) = \qquad (3)$$

$$\begin{cases} n_{\max_0} & |r| = 0, \\ n_0(x) = n_{\max_0}\sqrt{1 - 2\Delta(x/w)^{\alpha_0}} & 0 < |r| \leqslant R_0, \\ n_{\max_1} & |r| = R_0, \\ n_1(x) = n_{\max_1}\exp\{-\ln 2[2(x - x_0)^2/(hw)]\} & R_0 < |r| \leqslant R_1, \\ n_2 & R_1 < |r| \leqslant R_2. \end{cases}$$

where $n_{\max_0}$ and $n_{\max_1}$ are the highest refractive indices of the core and the cladding; n_0, n_1 and n_2 are refractive indices of various core and cladding regions; R_0, R_1 and R_2 are the respective radial distances; x is the local coordinate; w is the width of the region; α_0 is the profile parameter; Δ is the normalised refractive index difference [23]; x_0 is the peak position; and h is the normalised FWHM value of the Gaussian profile.

The bandwidth of an optical fibre determining the data rate is limited by chromatic dispersion D, which in turn is determined by the sum of the material dispersion D_m and the waveguide dispersion D_w [10]:

$$D = D_m + D_w = \left(-\frac{\lambda}{c}\frac{d^2 n}{d\lambda^2}\right) \qquad (4)$$

$$+ \left\{\frac{\lambda}{2\pi^2 cnW^2(\lambda, z)}\left[1 - \frac{2\lambda}{W(\lambda, z)}\left(\frac{3}{2}g_1(z)\lambda^{0.5} + 6g_2(z)\lambda^5\right)\right]\right\},$$

where $W(\lambda, z)$ is the mode field diameter; and g_1 and g_2 are the coefficients. By modifying the refractive index profile of a fibre we can control the waveguide dispersion contribution, and thereby we can modify the total dispersion as required. The bandwidth of a fibre is not only disturbed by chromatic dispersion, but also affected by PMD. PMD of a fibre can be calculated using the discrete model [24], which yields a mean value of the first-order PMD for a long fibre span. The average differential group delay (DGD) $\Delta\tau$ is proportional to the square root of the fibre length L:

$$\langle\Delta\tau\rangle = \sqrt{\frac{8}{3\pi}}\Delta\beta\sqrt{l}\sqrt{L}, \qquad (5)$$

where l is the coupling length.

The effective mode area of a fibre is given by the equation [25, 26]

$$A_{\text{eff}} = \frac{\left[\int_{-\infty}^{\infty}\int_{-\infty}^{\infty}|E(x,y)|^2\,dx\,dy\right]^2}{\int_{-\infty}^{\infty}|E(x,y)|^4\,dx\,dy}, \qquad (6)$$

where $E(x, y)$ is the optical mode field distribution. The value of A_{eff} is directly related to the nonlinearity of the optical fibre and the nonlinear coefficient γ is calculated using the equation [27]

$$\gamma = \frac{2\pi n_2}{\lambda A_{\text{eff}}}. \qquad (7)$$

Here n_2 is the nonlinear refractive index (typical value 3.1×10^{-20} m^2 W^{-1}) of silica fibre.

The mode field diameter (MFD) is an important parameter that is related to the optical field distribution of the fibre. The MFD is given by the equation [26]

$$d_{\text{eff}} = 2W = \frac{2}{\sqrt{\pi}}\sqrt{A_{\text{eff}}}. \qquad (8)$$

The MFD provides information about the fibre performance such as macro- and micro-bending losses. The bending loss of a fibre is calculated using the model described by Sakai and Kimura [28]. Macro-bending power loss is expressed as a function of the bending radius R_b in the form

$$\alpha_{\text{macro}} = \frac{\sqrt{\pi}\,P_{\text{cl}}/P}{2sr_{\text{co}}[K_{v-1}(W)K_{v+1}(W) - K_v^2(W)]}$$

$$\times \exp\left(-\frac{4}{3}\frac{R_b}{r_{\text{co}}}\frac{\Delta W^3}{V^2}\right)\left[W\left(\frac{WR_b}{r_{\text{co}}} + \frac{V^2}{2\Delta W}\right)^{1/2}\right]^{-1}, \qquad (9)$$

where

$$V = k_0 r_{\text{co}}\sqrt{n_{\max}^2 - n_{\text{cl}}^2}; \quad \Delta = \frac{n_{\max}^2 - n_{\text{cl}}^2}{2n_{\max}^2}; \quad W = r_{\text{co}}\sqrt{\beta^2 - (k_0 n_{\text{cl}})^2};$$

r_{co} is the fibre core radius; $n_{\max}$ is the maximum value of the refractive index; n_{cl} is the index of the cladding; β is the propagation constant of the mode; k_0 is the wave number in vacuum; v is the azimuthal mode number; $s = 2$ (if $v = 0$) or $s = 1$ (if $v \neq 0$); and K_v is the modified Bessel function of the second kind of order v.

Micro-bending loss is a radiative loss in fibre resulting from mode coupling caused by random micro-bends, which are repetitive small-scale fluctuations in the radius of curvature of the fibre axis. An approximate expression for the micro-bending loss is given in [29] and has the form

$$\alpha_{\text{micro}} = A(k_0 n_{\text{co}} d_n)^2 (k_0 n_{\text{co}} d_n^2)^{2p}, \qquad (10)$$

where A is the constant; d_n is the near field diameter; n_{co} is the refractive index of the fibre core; and p is the exponent in the power law.

The splice loss is also an important parameter in the fibre design. Any index-of-refraction mismatch at any point in the interface between the highly nonlinear fibre (HNLF) and single-mode fibre (SMF) will produce reflection and refraction of the light incident at that point and induce the splice loss. For splice loss calculations, we have assumed that the mode field of SMF is nearly Gaussian. The coupling losses for the splice connectors can be calculated by evaluating the coupling between two misaligned MFD of Gaussian beams based on the model that is given by Miller and Kaminow [30]:

$$\alpha_{\text{splice}} = -10\log\left[\left(\frac{16n_{\text{co}}^2 n_{\text{mat}}^2}{(n_{\text{co}} + n_{\text{mat}})^2}\right)\frac{\sigma}{q}\exp\left(\frac{-\rho u}{q}\right)\right], \qquad (11)$$

where

$$\rho = \frac{(kw_1)^2}{2}; \quad q = G^2 + \frac{(\sigma + 1)^2}{4};$$

$$u = (\sigma + 1)F^2 + 2\sigma FG\sin\theta + \sigma\left(G^2 + \frac{\sigma + 1}{4}\right)\sin^2\theta;$$

$$F = \frac{x}{kw_1^2}; \quad G = \frac{z}{kw_1^2}; \quad \sigma = \left(\frac{w_2}{w_1}\right)^2; \quad k = \frac{2\pi n_{\text{mat}}}{\lambda};$$

n_{mat} is the refractive index of the medium between the two fibres; w_1 and w_2 are the near-field mode radii of transmitting and receiving fibres; x and z are the lateral and longitudinal offsets; and θ is the angular misalignment.

The cutoff wavelength λ_{cut} for any mode is defined as the maximum wavelength at which that mode will propagate:

$$\lambda_{\text{cut}} = \frac{2\pi R_0}{V_{\text{cut}}}\sqrt{n_{\text{co}}^2 - n_{\text{cl}}^2}, \qquad (12)$$

where R_0 is the fibre core radius; and $V_{\text{cut}} = 2.405$ is the parameter defined analytically for specified fibre profiles. We have two different approaches for finding the cutoff wavelength λ_{cut} for the fundamental mode as shown in Table 1. The theoretical cutoff wavelength above which the given mode cannot propagate is calculated using the general numerical mode-solvers. An 'estimated ITU-T' cutoff value is obtained by emulating the actual experimental cutoff measurements, as described in [31].

Refractive index profile based fibre design and optimisation are carried out with the help of the built-in numerical fibre mode-solver of Optifibre tool by the matrix method. It will find linearly polarised modes by an exact method that uses radial transfer matrices. This method is more accurate, especially in the calculation of dispersion and other derivatives with wavelength. Here, the design optimisation is done by parameter scanning, i.e., on the basis of the parametrical calculations of some fibre characteristic versus certain technological properties or quantities of the fibre design (for example, the core/cladding refractive index difference, the spatial width or some region, etc). It predicts automatically how any given fibre could be optimised versus a design goal, for example zero dispersion and minimal mode area.

By applying the parametric scanning and the matrix method (3), it is found that newly designed HN-UFF (Fibre C) offers its optimum performance at the below mentioned conditions:

$a = 62.5$ µm (total fibre radius);

$R_0 = 2.025$ µm, $a_0 = 2.025$ µm;

$R_1 = 1.1$ µm, $a_1 = 3.125$ µm;
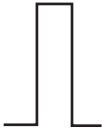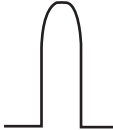
$R_2 = 59.375$ µm, $a = 62.5$ µm; $\qquad (13)$

$n_0(x) = n_{\text{max}_0}\sqrt{1 - 2\Delta_0(x/w)^{\alpha_0}}$ (alpha-peak profile);

$n_1(x) = n_{\text{max}_1}\exp\left\{-\ln 2\left[\frac{2(x - x_0)}{hw}\right]^2\right\}$ (Gaussian profile);

Table 1. Performance parameters of optimally designed Fibre A, Fibre B and Fibre C.

Parameters	Fiber A	Fiber B	Fiber C
Index profile			
Zero dispersion wavelength λ_{ZDW}/µm	1.4205	1.5673	1.487 and 1.9857
Dispersion slope (at $\lambda = \lambda_{\text{ZDW}}$)/ps nm^{-2} km^{-1}	0.04753	0.3038	0.02476 at $\lambda_{\text{ZDW}} = 1.487$ µm, 0.0068 at $\lambda_{\text{ZDW}} = 1.9857$ µm
Dispersion variation over S, C, L and U bands (at $\lambda = 1.47$–1.98)/ps km^{-1} nm^{-1}	from 2.25 to 15.85 and 5.06 at $\lambda = 1.55$ µm	from −3.26 to 10.34 and −0.6 at $\lambda = 1.55$ µm	from −0.22 to 1.61 and 1.02 at $\lambda = 1.55$ µm
MFD (at $\lambda = 1.55$ µm)/µm	4.465	4.41	4.211
A_{eff} (at $\lambda = 1.55$ µm)/µm^2	16	15.6	13.32
Nonlinearity coefficient (at $\lambda = 1.55$ µm)/W^{-1} km^{-1}	7.93	8.055	9.43
First-order PMD/ps	0.102	0.058	0.051
Splice loss (at $\lambda = 1.55$ µm)/dB	0.49	0.77	0.11
Bending loss (at $\lambda = 1.55$ µm)/dB	$\alpha_{\text{macro}} = 6.425 \times 10^{-21}$ $\alpha_{\text{micro}} = 2.33 \times 10^{-2}$	$\alpha_{\text{macro}} = 1.674 \times 10^{-16}$ $\alpha_{\text{micro}} = 4.116 \times 10^{-2}$	$\alpha_{\text{macro}} = 2.404 \times 10^{-14}$ $\alpha_{\text{micro}} = 6.9 \times 10^{-3}$
Calculated cutoff wavelength/µm	1.512 (ITU-T = 1.479)	1.402 (ITU-T = 1.375)	1.2759 (ITU-T = 1.2613)

$n_2 = 1.44692$, $n_{\max_0} = 1.475$, $n_{\max_1} = 1.445$, $\Delta_0 = 0.65\%$;

$\alpha_0 = 3.5$, $h = 14$, $x_0 = 2.025$.

Due to the symmetrical nature of the fibre, we consider here only the refractive index profile for half a fibre in terms of its radii (a_0 and a_1 are the cumulative radii of the regions of width R_0 and R_1, respectively).

3. Implementation of the proposed optimised HN-UFF fibre

Initially, the design of proposed HN-UFF was started with a very high refractive index of the core having a radius R_0 for a fibre with a single cladding having a radius R_2 (without R_1 region). With increasing index difference between the core and cladding, the effective area is reduced with increasing nonlinearity coefficient [32] and the dispersion slope is shifted towards lower wavelengths. Reduction of the effective area can be achieved by decreasing the MFD [25, 26]. The refractive index profile of a specific region is optimised by successive iterations of the region parameters with the help of a numerical fibre mode-solver by the matrix method. First (see Fig. 1b), we calculated the fibre performance for the optimised index profile in the R_0 and R_2 regions without the alpha parameter and in the R_1 region (Fibre A). The optimum fibre performance parameters for Fibre A are obtained at a maximum refractive index of the core, $n_{\max_0} = 1.475$, and a radius $R_0 = 2.025$ μm. Usually a high refractive index of the fibre is obtained by adding germanium to silica and a lower refractive index is obtained by adding fluorine [33]. This high core–cladding index difference (step index) ensures our ultimate aim of a low effective area $A_{\mathrm{eff}} = 16$ μm^2 and a respective higher nonlinear coefficient $\gamma = 7.93$ W^{-1} km^{-1}. The obtained effective MFD of this fibre is 4.465 μm. The designed fibre also has a very low bending loss and splice loss (see Table 1). We have attained λ_{ZDW} at about 1.4205 μm and the dispersion of this fibre is 5.06 ps nm^{-1} km^{-1} at 1.55 μm with a dispersion slope of 0.04753 ps nm^{-2} km^{-1}. By optimising the width of the core to 2.025 μm, we have also ensured fibre's fundamental mode (LP$_{01}$) operation. The cutoff wavelength of this fibre in this case is as high as 1.512 μm. This combination of the dispersion slope and cutoff wavelength will limit the bandwidth utilisation of Fibre A.

To pursuit low dispersion while designing a high bandwidth fibre, a significant consideration should not solely be on material dispersion but also on waveguide dispersion. Also, enough attention should be given to its associated specific field configuration of electromagnetic radiation within the fibre. Concentration of power near the core–cladding interface will have different dispersive characteristics than the power in the core. Waveguide dispersion varies with physical characteristics of fibre, such as the core radius, the α_0 value for a graded structure, the relative index difference and the transmission wavelength. Optimising the above parameters will lead to a change in waveguide dispersion, opposite to that of material dispersion. Therefore, there will be room for the design of fibre with waveguide dispersion that would exactly cancel the material dispersion and finally a near-zero dispersion could be obtained [19].

Now we introduce the parameter α_0 for the core as given in Eqn (3) in order to improve the performance of the fibre

named Fibre B. At an optimal $\alpha_0 = 3.5$, the zero dispersion wavelength shifts to the longer wavelength side up to 1.5673 μm with decreasing dispersion slope down to 0.3038 ps nm^{-2} km^{-1} without compromising the bending loss and splice loss. The MFD is reduced to 4.41 μm and the resultant effective area due to the contribution of R_0 and R_2 regions is 15.6 μm^2. Thus, the fibre nonlinearity is also slightly increased to 8.055 W^{-1} km^{-1}. A very minimum level of macro- and micro-bending loss is obtained, such as 1.67×10^{-16} and 4.116×10^{-2} dB km^{-1}, respectively, for 12-mm diameter bending per turn. With increasing α_0, the cutoff wavelength of this fibre shifts towards the lower wavelength and reaches 1.402 μm for the optimum value of α_0.

But still Fibre B does not possess perfect flattened dispersion characteristics (or a wide spectrum of normal zero dispersion). The overall dispersion characteristic of the fibre is controlled by modifying the waveguide dispersion contribution by including the R_1 region with a depressed cladding index. This new design of the fibre index profile is named Fibre C (see Fig. 1a). This inclusion of the R_1 region with a depressed cladding index [12, 34] also reduces the effective area of the fibre and perfectly flattens the dispersion curve down to zero. In addition, it reduces the bending loss of the fibre too [35]. The region R_1 is also optimised through simulations to obtain an optimised HN-UFF for future optical communication. From the successive iterations, the obtained optimum maximum refractive index of the R_1 region is $n_{\max} = 1.445$, the width of the R_1 region is 1.1 μm and the FWHM of the Gaussian profile is 14. At these optimised parameters the waveguide and material dispersions can cancel each other, which leads to a flattened zero dispersion over the wide range of the spectrum. The measured bending loss is also acceptable at the optimised (region R_1) cladding refractive index and the cladding width.

The proposed optimal index profiled Fibre C design exhibits an improved overall performance such as ultra-flattened dispersion characteristics with a very low splice loss and ability to operate only in the fundamental LP$_{01}$ mode. The optimised alpha-peak profile is in the core and the Gaussian profile is in the depressed cladding region [see Eqn (17)]. This index profile will allow a finer optical confinement within the core with a reduced MFD of 4.21 μm and an increase in respective nonlinearity. These effects lead to an improvement in the splice loss as compared to that in Fibre B. However, the bending loss can be controlled as shown in Fig. 2. Macro- and micro-bending losses of Fibre C are 2.404×10^{-14} and 6.9×10^{-3} dB km^{-1}, respectively. The splice loss is also very low and equal to 0.11 dB at 1.55 μm. The values of λ_{ZDW} of this fibre are 1.487 and 1.9857 μm, which can extend the usable bandwidth to the entire S, C, L and U bands with a maximum dispersion value of 1.61 ps km^{-1} nm^{-1}. This fibre has a very low theoretical cutoff wavelength of 1.2759 μm with a very good nonlinear coefficient of 9.43 $^{-1}$ km^{-1}.

Figure 3a and 3b clearly show the effect of $n_{\max}$ of the R_1 region and its width on total dispersion characteristics of Fibre C. As the refractive index of the region is increased, the dispersion slope of the proposed fibre is increased and a perfect flattened dispersion value is obtained at $n_{\max} = 1.445$. At the same time, an increase in the R_1 region width leads to a shift of the total dispersion curve to positive values (at an optimal width of 1.1 μm), because the total dispersion in this case is nearer to zero (anonymous dispersion) over a wide range of the spectrum. Figure 3c also shows the optimisation
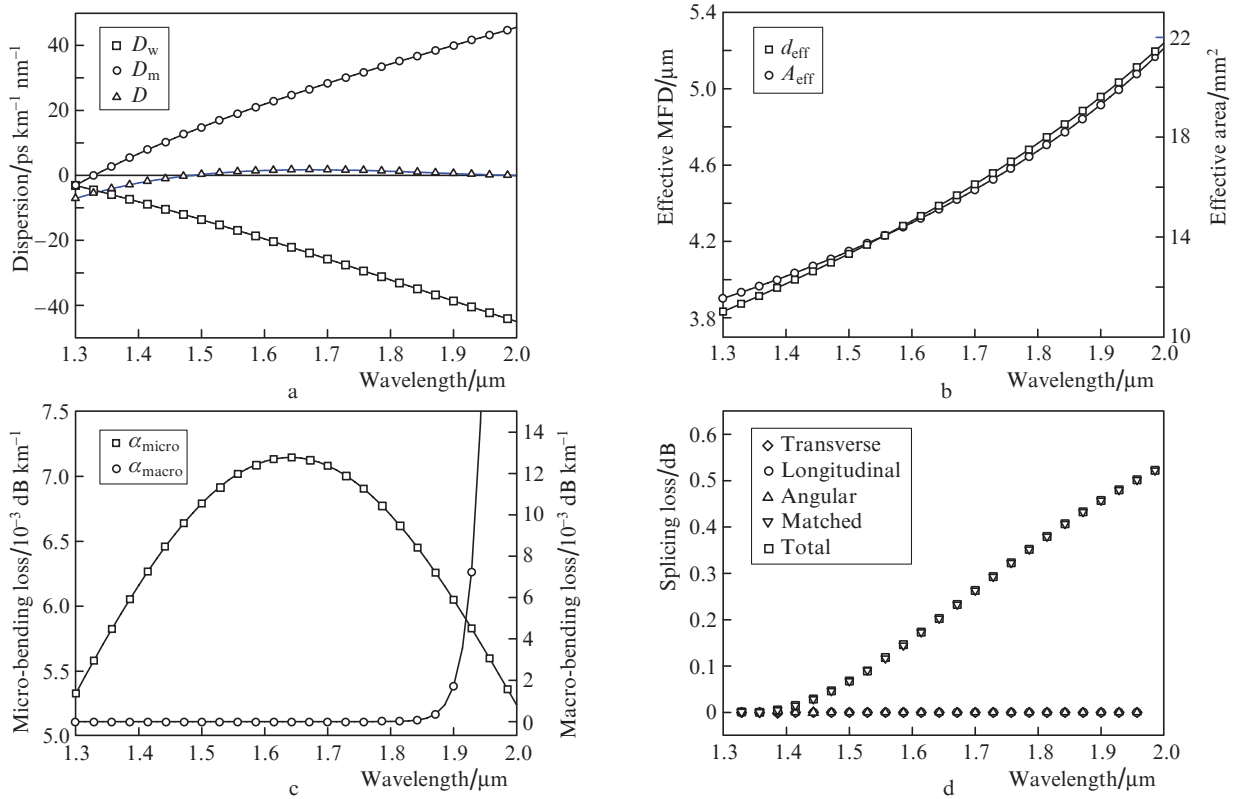
Figure 2. Dependences of (a) dispersion, (b) MFD, (c) bending loss and (d) splice loss on the wavelength for Fiber C.
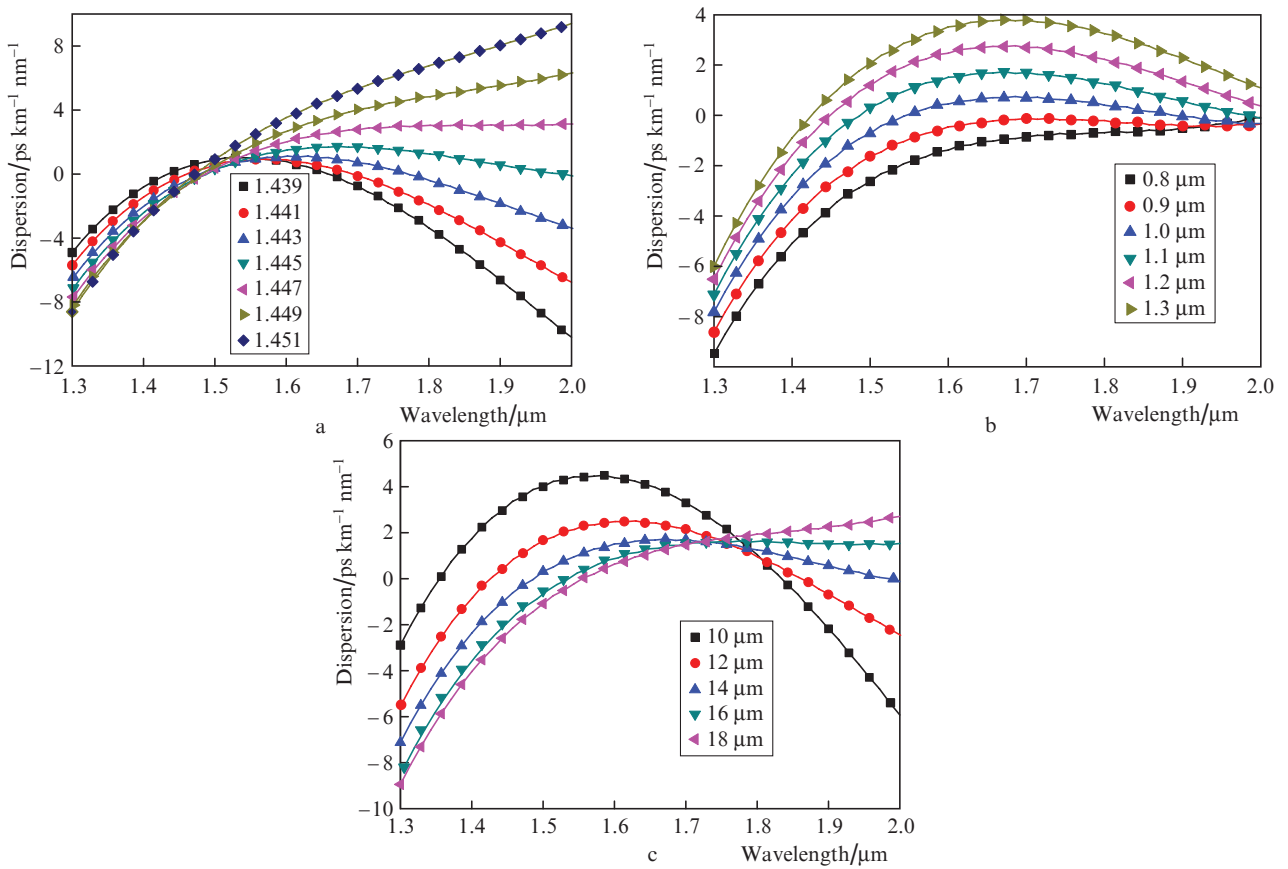

Figure 3. Wavelength dependence of the Fibre C dispersion at different values of (a) n_{max}, (b) R_1 region width and (c) normalised FWHM h of the Gaussian profile in the R_1 region.
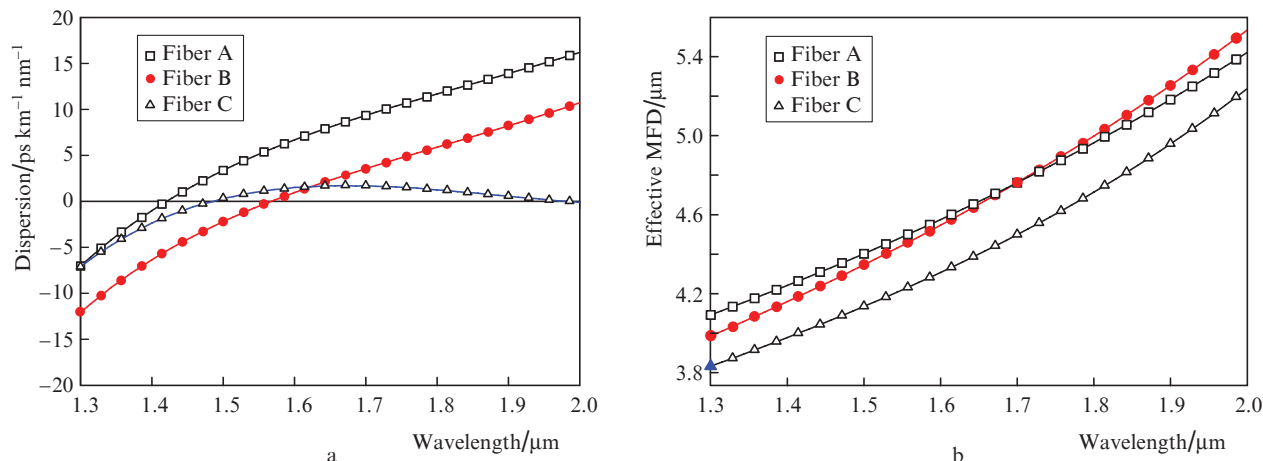
Figure 4. Wavelength dependences of (a) dispersion and (b) effective MFD for Fibre A, B and C.

of the Gaussian profile FWHM h in the R_1 region. The perfect dispersion flatness is reached at $h = 14$. The measured total dispersion and effective MFD of Fibre A, B and C are compared in Fig. 4. Fibre C demonstrates a superior performance in dispersion flattening and increased nonlinearity resulting from the reduced MFD. The Gaussian profile of the R_1 region in Fibre C improves the confinement of the field distribution and reduces the MFD as compared to Fibre A and B. Figure 5 shows 3D plots of the mode field distribution of Fibre B and our optimised Fibre C. One can see that Fibre C with an alpha-peak profile of the graded index in the core and a Gaussian profile in the R_1 region of the cladding is indeed an optimised highly nonlinear ultra-flattened dispersion fibre. Inclusion of the R_1 region in the Fibre C design reduces the cutoff wavelength to 1.2759 µm (ITU-T = 1.2613 µm) and ensures the fibre operation only with the fundamental linearly polarised PL_{01} mode. At the same time, Fibre B without the R_1 region operates at LP_{01} and LP_{11} modes (Fig. 5a). The elimination of the LP_{11} mode in Fibre C also significantly contributes the fibre dispersion flattening.
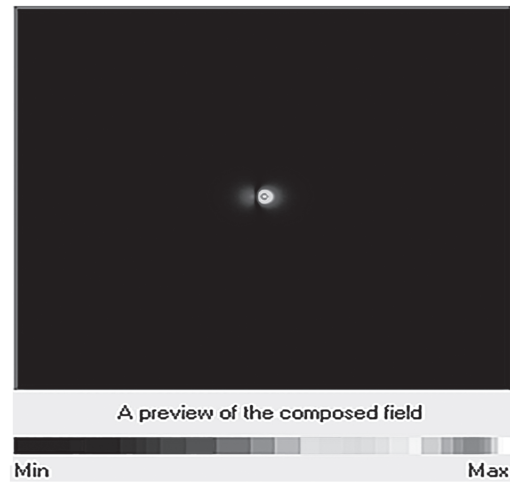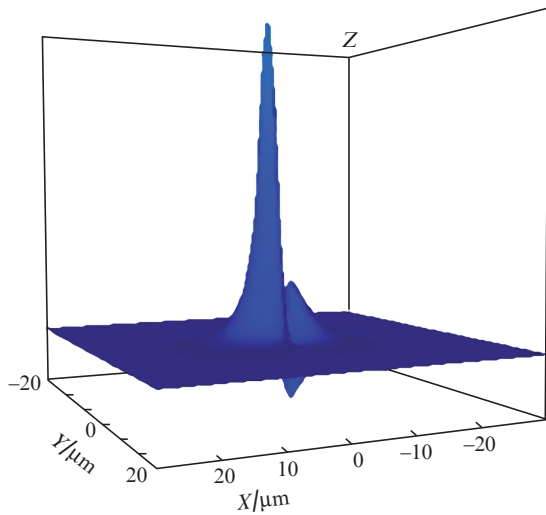
The optimised parameters of Fibre A, B and C are listed in Table 1. Fibre C has two wavelengths λ_{ZDW} with a very low dispersion slope in between, so that it can support optical signal processing in a broad spectral range. The dispersion variation in the HNLF over S, C, L, U bands and beyond is also very low as compared to the previously reported results [5, 12, 25, 26, 36–39]. Our proposed Fibre C exhibits a very good effective area and nonlinear coefficient. Even though this Fibre C has a slightly smaller nonlinearity of 9.43 W^{-1} km^{-1} than that of the previously reported HNLF, a perfect phase matching condition between the signals is obtained due to an ultra-flattened normal zero dispersion characteristic of our Fibre C, which in turn allows efficient wavelength conversion in optical networks using the FWM technique and also supercontinuum generation.

4. Results and discussion

Plasma-activated chemical vapour deposition (PACVD) manufacturing technology is the most suitable for fabricating a fibre with a hyperfine refractive index profile. Compared to an outside thermally activated method, PACVD technology

offers an extremely thin layer deposition (deposition rate of 0.5–1 g min^{-1}) with a high efficiency ($\sim 100\%$ for SiO_2 and $80\% - 100\%$ for GeO_2) due to different reaction kinetics. Thus, hundreds of cycles are performed, and less than one micrometre thick layers are deposited, allowing a very good control of the refractive index profile in the preform [40, 41, 42], as in equation (17). The optimised design of fibre [see (17)] exhibts the optimal performances as listed in Table 1. Our optimal Fibre C design (HN-UFF) ensures a very low dispersion and a wide spectral range of flatted dispersion (Fig. 6). The proposed fibre has two zero dispersion wavelengths λ_{ZDW} (at 1.487 and 1.9857 µm) with a maximum dispersion variation of 1.61 ps km^{-1} nm^{-1} between these wavelengths. The measured dispersion slope at $\lambda_{ZDW} = 1.487$ µm is 0.02476 ps nm^{-2} km^{-1}. Figure 6 clearly shows that at wavelengths in the range from 1.53 to 2 µm, the measured dispersion slope varies in a narrow interval between +0.01 to –0.01. This lower value of the dispersion slope demonstrates the quality of the dispersion curve flatness. The optimised Fibre C also has $A_{eff} = 13.32$ $µm^2$ and $\gamma = 9.43$ W^{-1} km^{-1}. Further improvement in the nonlinear coefficient is also possible, but bending and splice losses have to be compromised. Besides, it can affect the flattened dispersion characteristics.

The PMD is calculated using a discrete model. The fibre length L is assumed equal to 1 km and the coupling length is $l = 20$ m, the intrinsic perturbation of the core ellipticity is $\xi = 0.01$ and the differential thermal expansion is equal to 6.5×10^{-8}. Our optimised fibre has a very low first-order PMD value of 0.051 ps. Under perfect splicing (without external misalignment) with SMF having a MFD of 9.8 µm and a matching index within the cladding, our optimal HN-UFF has a very low splice loss of 0.11 dB. The index profile in the R_1 region of Fibre C, which is next to the core, is very low. This maximum index difference between the core and the cladding will strongly confine the light into the core and prevents its leaking to the cladding [12, 34]. Thus, the bending loss can be ignored even in the case of a coiled fibre cable [14]. Therefore, the measured macro- and micro-bending losses at 1.55 µm for our optimised Fibre C are as low as 2.404×10^{-14} and 6.9×10^{-3} dB km^{-1}, respectively, even in the case of a 12-mm bending diameter. To estimate the macro-bending loss, use was made of the formula [30] applicable to any mode at an arbitrary-index profile. The theoretical cutoff wave-

a
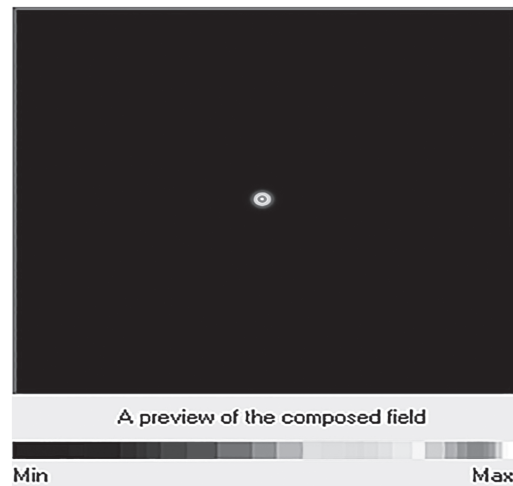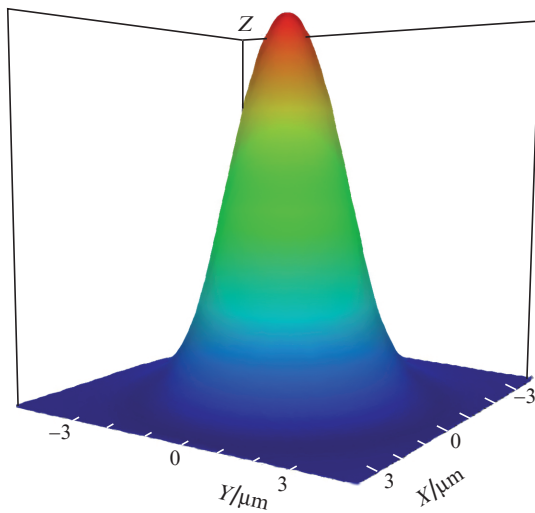
b

Figure 5. Mode field distribution in (a) Fibre B and (b) optimised Fibre C.
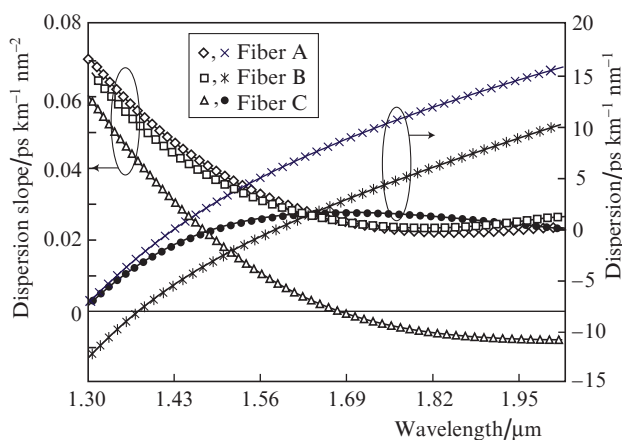

Figure 6. Wavelength dependences of dispersion and the dispersion slope for Fibre A, B and C.

length of Fibre C, calculated using the general numerical mode solvers, is 1.2759 μm, while the 'estimated ITU-T' cutoff value is 1.2613 μm. Our optimised Fibre C operates at the fundamental mode (LP_{01}) only due to the very low cutoff wavelengths and hence it can be efficiently utilised in S, C, L, U bands and beyond.

Table 2 shows the supported modes in our designed Fibre A, B and C along with the mode index and calculated field. The values in the 'Power' column correspond to the squared sum of the real and imaginary parts and have the meaning of the usual coupling coefficients of a particular mode. To calculate these above values, the launching input beam with a Gaussian profile (FWHM = 10 μm) and a polar angle of 0° with respect to fibre axis has a coupling coefficient of 0.34968 for the LP_{01} mode, which is approximately equal to that of Fibre A and B, but the LP_{11} influence on fibre propagation characteristics is eliminated. By reducing the FWHM of the launching Gaussian field, the coupling coefficient is increased.

Table 2. Modes of the designed fibre profiles with a power coupling coefficient.

Fibre	Supported mode and mode index	Power coupled to mode		
		Mode field amplitude	Mode field phase	Power (coupling coefficient)
Fiber A	LP_{01}; 1.4643102	0.61792	0	0.38182
	LP_{11}; 1.4501719	1.6544×10^{-16}	0	2.7369×10^{-32}
Fiber B	LP_{01}; 1.4624935	0.61681	0	0.38046
	LP_{11}; 1.4481877	2.6749×10^{-16}	0	7.1552×10^{-32}
Fiber C	LP_{01}; 1.4620085	0.59134	0	0.34968

The anomalous dispersion region is of interest for such nonlinear-optical applications as soliton propagation, optical phase conjugation and supercontinuum generation. Particularly, supercontinuum generation requires several zero dispersion wavelengths and also a large separation between them. Thus, our aim was to flatten the dispersion at a minimal positive value (near zero) over the wide range of the spectrum as well as to obtain several zero dispersion wavelengths in order to utilise the entire spectrum (from 1.48 to 1.98 μm) for nonlinear signal processing. In our design, 500-nm wavelength spacing in the optical spectrum has the dispersion variation from 0 to 1.61 ps km^{-1} nm^{-1}, which means that the entire spectrum can be efficiently used. By reducing the core diameter, we can increase the waveguide negative dispersion and then at an optimised value the total dispersion curve lies exactly on the zero dispersion line. However, these modifications limit the bandwidth utilisation to below 250 nm and affect other parameters such as bending and splice losses.

5. Conclusions

We have designed an optimised highly nonlinear fibre with an ultra-flattened dispersion characteristic. The optimised Fibre C exhibits the dispersion flatness over 500 nm of S, C, L, U bands and beyond with a dispersion variation between 0 to 1.61 ps km^{-1} nm^{-1}. The designed fibre has two wavelengths λ_{ZDW} equal to 1.487 and 1.9857 μm. The calculation results show that the optimised Fibre C has a high nonlinear coefficient (9.43 W^{-1} km^{-1}) and a very low splice loss (0.11 dB). The mean value of the first-order PMD of our designed fibre is as low as 0.051 ps. Fibre C ensures a very large bandwidth of operation due to its flattened normal zero dispersion over a wide range of the spectrum and very low cutoff wavelength of 1.2613 μm. The macro- and micro-bending losses are 2.404×10^{-14} and 6.9×10^{-3} dB km^{-1}, respectively. Therefore, the bending loss can be ignored even in the case of a fibre cable that is wound as a coil in compact systems. Our proposed design is suitable for many nonlinear applications such as fibre lasers emitting at different wavelengths, parametric amplification, wavelength conversion, optical regeneration, optical sampling, pulse compression, and mainly for supercontinuum generation.

References

1. Saruwatari M. *IEEE J. Sel. Top. Quantum Electron.*, **6** (6), 1363 (2000).
2. Wu X., Huang H., Wang J., Wang X., Yilmaz O.F., Nuccio S.R., Willner A.E. *Conf. Lasers and Electro-Optics (CLEO) and Quantum Electronics and Laser Science (QELS)*, **1–2**, 16 (2010).
3. Wang D., Cheng T.-H., Yeo Y.-K., Xu Z., Wang Y., Xiao G., Liu J. *IEEE J. Lightwave Technol.*, **28** (24), 3497 (2010).
4. Ophir N., Chan J., Padmaraju K., Biberman A., Foster A.C., Foster M.A., Lipson M., Gaeta A.L., Bergman K. *IEEE Photon. Technol. Lett.*, **23** (2), 73 (2001).
5. www.oelabs.com/.
6. Hirano M., Nakanishi T., Okuno T., Onishi Masashi. *IEEE J. Sel. Top. Quantum Electron.*, **15** (1), 103 (2009).
7. Weber H.G., Nakazawa M. *Ultrahigh-speed Optical Transmission Technology* (Berlin: Springer, 2007) pp 141–165.
8. Inoue K. *IEEE J. Lightwave Technol.*, **10** (11), 1553 (1992).
9. Bass M., van Stryland E.W. *Fiber Optics Handbook: Fiber, Devices, and Systems for Optical Communications* (New York: McGraw-Hill, 2002).
10. Shizhuo Yin, Kun-Wook Chung, Hongyu Liu, Kurtz P., Reichard K. *Opt. Commun.*, **177** (1837–6), 225 (2000).
11. Wandel M., Kristensen P. *J. Opt. Fiber Commun.*, **3** (1), 25 (2006).
12. Li Ming-Jun, Li Shenping, Daniel A.Nolan. *Proc. SPIE Int. Soc. Opt. Eng.*, **6025**, 602503 (2006).
13. Ramachandran S., Ghalmi S., Nicholson J.W., Yan M.F., Wisk P., Monberg E., Dimarcello F.V. *Opt. Lett.*, **31** (17), 2532 (2006).
14. Okuno T., Hirano M., Nakanishi T., Onishi M. *SEI Tech. Rev.*, **62**, 34 (2006).
15. Camerlingo A., Feng X., Poletti F., Ponzo G.M., Parmigiani F., Horak P., Petrovich M.N., Petropoulos P., Loh Wei H., Richardson D.J. *Opt. Express*, **18** (15), 15747 (2010).
16. Feng X., Shi J., Ponzo G.M., Poletti F., et al. *Proc. ECOC* (Geneva, 2011) paper We.10.P1.05.
17. Poletti F., Feng X., Ponzo G.M., Petrovich M.N., Loh W.H., Richardson D. *Opt. Express*, **19** (1), 66 (2011).
18. Chamberlain G.E., Day G.W., Franzen D.L., Gallawa R.L., Kim E.M., Young M. *NBS* (1983) p. 225.
19. Carnevale Anthony, Paek Un-Chul., Peterson George E. Patent US 4412722A (Nov. 1, 1983).
20. Ma Daiping, Smith David Kinney. Patent US 2001/0001624 A1 (May 24, 2001).
21. Seraji F.E., Kiaee R. *Intern. J. Opt. Appl.*, **4** (2), 62 (2014).
22. Rostami A., Makouei S., in *Advances in Solid State Circuit Technologies* (ISBN, InTech, 2010) pp 107–140.
23. https://optiwave.com/category/resources/publications/.
24. Bruyère F. *Ph.D. Diss.* (University of Paris XI Orsay, 1994).
25. Shashi Kant, Hrudayaranjan Sahu, Abhay Arora. *Proc. the 55th IWCS/Focus* (Providece, Rhode Island, USA, 2006) pp 330–333.
26. Jong-Kook Kim. *Ph.D. Thesis* (Virginia Polytechnic Institute and State University, Blacksburg, VA, 2005).
27. Selvendran S., Sivanantharaja A., Kalaiselvi K., Esakkimuthu K. *Opt. Quantum Electron.*, **45** (2), 135 (2013).
28. Sakai J., Kimura T. *Appl. Opt.*, **17** (10), 1499 (1978).
29. Petermann K. *Electron. Lett.*, **20** (3), 107 (1976).
30. Miller S.E., Kaminow I.P. *Optical Fiber Telecommunications II* (CA: Acad. Press, 1988).
31. *Definition and Test Methods for the Relevant Parameters of Single Mode Fibers.* ITU-T Rec. G.650 (1993).
32. Agrawal G.P. *Nonlinear Fiber Optics* (Acad. Press, 2007).
33. Masanori Takahashi, Jiro Hiroishi, Ryuichi Sugizaki, Yuki Taniguchi. Patent US 7006742 B2 (Feb 28, 2006).
34. Sillard P., Molin D. Patent US 2011/0188826 A1 (Aug. 4, 2011).
35. Dana Craig Bookbinder, Ming-Jun Li, Pushkar Tandon. Patent US 8588569 B2 (Nov. 19, 2013).

36. Saini T.S., Baili A., Kumar A., Cherif R., Zghal M., Sinhaa R.K. *Mod. Opt.*, **62** (19), 1570 (2015).
37. Saini T.S., Kumar A., Sinha R.K. *J. Lightwave Technol.*, **33** (18), 3914 (2015).
38. Agrawal A., Tiwari M., Azabi Y.O., Janyani V., Rahman B.M., Grattan K.T. *J. Mod. Opt.*, **60** (12), 956 (2013).
39. Wijeratne I.N.M., Kejalakshmy N., Agrawal A., Rahman B.M.A., Grattan K.T.V. *IEEE Photon. J.*, **4** (2), 357 (2012).
40. Kyunghwan Oh., Un-Chul Paek. *Silica Optical Fiber Technology for Devices and Components: Design, Fabrication, and International Standards* (John Wiley & Sons, 2012) p. 96.
41. Beck B. *Photon. Spectra*, **39** (12), (2005).
42. Sanghera J.S., Aggarwal I.D. *Infrared Fiber Optics* (CRC Press, 1998) pp 43–45.